Microstructure Evolution of Multicomponent γ′-Strengthened Co-Based Superalloy at 750 °C and 1000 °C with Different Al and Ti Contents

YI ZHANG, HUADONG FU, XIAOZHOU ZHOU, YUHENG ZHANG, HONGBIAO DONG, and JIANXIN XIE

Three novel Co-30Ni-$(7 - 1.5x)$Al-2W-1.5Mo-1Ta-$(3.5 + 0.7x)$Ti-12Cr -0.1Hf-0.08C-0.08B-0.4Si-0.01Zr (x = 0, 1, 2 at. pct) γ′-strengthened wrought Co-based superalloys with varying concentrations of Al and Ti were investigated to clarify the effects of the Al and Ti concentration on the microstructural stability at 750 °C and 1000 °C. The results show that the 7Al-3.5Ti and 5.5Al-4.2Ti alloys maintain a γ/γ′ two-phase microstructure after aging at 1000 °C for 600 hours, but the 4Al-4.9Ti alloy forms a $\eta(D0_{24})$-$(Co,Ni)_3$Ti phase after aging at 1000 °C for 312 hours. There exist stacking faults in the γ′ phase adjacent to the $D0_{24}$ needles, which form during the aging process, and the growth of the $\eta(D0_{24})$ phase is controlled by the diffusion of W. The γ′ phase and $\eta(D0_{24})$-$(Co,Ni)_3$Ti phase exhibit the following OR: $\langle 11\bar{2}0 \rangle \{0001\}\eta \| \langle 110 \rangle \{111\}\gamma\prime$. All the alloys possess good intermediate-temperature microstructural stability, with γ/γ′ two phases after aging at 750 °C for 1500 hours. With increasing Ti content and decreasing Al content, the coarsening rate of γ′ at 1000 °C first decreases and then increases; however, it gradually decreases at 750 °C. This difference in the coarsening behavior is attributed to the interaction of the interfacial energy, diffusion of the solute atoms and coherent stress.

I. INTRODUCTION

NOVEL γ′-hardened Co-Al-W-based alloys (Hereinafter denoted as novel Co-based superalloys) which are expected to develop into a new generation of high-temperature structural materials, shows good solidification characteristics and mechanical properties compared with nickel-base superalloys.[1–3] In addition, the low γ′ solvus temperature and high solidus temperature of these novel Co-based superalloys are beneficial for producing wrought superalloys with a large hot processing window by casting and forging.

Remarkable efforts have been made to clarify the effects of alloying element additions on the microstructural stability and mechanical properties of novel Co-based superalloys with low-order alloying additions.[4–10] However, research focusing on multicomponent γ′-strengthened wrought novel Co-based superalloys is still insufficient, especially for microstructural stability during long-time aging. With the goal of improving the mechanical properties and oxidation resistance, Neumeier et al.[11,12] developed a high-performance multicomponent novel wrought Co-based superalloy by a cast and wrought processing approach, which possessed a much better creep property and oxidation resistance compared with Udimet 720Li. Knop et al.[13] produced a new polycrystalline CoNi-based superalloy (V208C) by the powder metallurgy route, which showed a better high-temperature strength compared with MarM247. Focusing on reducing the mass density of multicomponent alloys, our group has also made some progress in reducing the mass density of multicomponent Co-based alloys.[14] The abovementioned reports provide good guidance for further developing novel wrought Co-based superalloys with high performance.

In addition to the mechanical properties of the alloys after standard heat treatments, the evolution of the microstructure (including the γ′ phase coarsening and

YI ZHANG, HUADONG FU, XIAOZHOU ZHOU, YUHENG ZHANG, and JIANXIN XIE are with the Beijing Advanced Innovation Center of Materials Genome Engineering, University of Science and Technology Beijing, Beijing 100083, P.R. China and also with the Key Laboratory for Advanced Materials Processing of Ministry of Education, Institute for Advanced Materials and Technology, University of Science and Technology Beijing, Beijing 100083, P.R. China. Contact e-mail: hdfu@ustb.edu.cn HONGBIAO DONG is with the Beijing Advanced Innovation Center of Materials Genome Engineering, University of Science and Technology Beijing.

the formation of TCP phases) with increasing servicing time can severely affect their performance under a servicing environment, which can directly lead to the failure of hot-end components. The novel Co-based superalloys possess a narrow γ/γ' two-phase field and a large amount of W,[1] which can promote the formation of β-B2,[15] μ-Co$_7$W$_6$ and χ-Co$_3$W.[16,17] Although relevant research has shown that the Ni addition can increase the γ/γ' two-phase field of Co-based superalloys,[4,10] the TCP phase can still form during prolonged heat treatment in multicomponent CoNi-based superalloys.[18,19] Therefore, it is crucial to study the microstructural stability at high temperature for the application of new novel alloys.

Our recent work revealed that the mechanical properties of the novel wrought Co-based superalloys can be improved by replacing 1.5 at. pct Al with 0.7 at. pct Ti on the premise of maintaining a large processing window and good hot deformation property.[20] This work aims to further identify the effects of relevant Al and Ti content on the microstructural stability at 1000 °C and 750 °C. Moreover, the experimental results are compared and discussed with those calculated using the commercial software Pandat combined with the latest Co-based database (PanCo-2019-TH). These results may provide guidance for the development of novel wrought Co-based superalloys with high performance and microstructural stability.

II. MATERIALS AND METHODS

Based on our previous research,[20] this paper further investigated the microstructural stability of three alloys with different Al and Ti contents at 1000 °C and 750 °C. Herein, the alloys will be referenced under their relevant Al and Ti contents as 7Al-3.5Ti, 5.5Al-4.2Ti and 4Al-4.9Ti. Table I shows the compositions of the experimental alloys.

Three button ingots weighing 50 g were prepared by arc melting in an argon atmosphere, and each ingot was remelted 8 times. The purity of all raw elements was 99.99 pct by mass or higher, and the total mass loss of the master alloys during arc melting was less than 0.1 pct. Alloy samples were encapsulated in quartz tubes that were back-filled with argon, following a two-step solution heat treatment of 1110 °C for 6 hours + 1190 °C for 10 hours. Bulk compositions were measured by a JXA8230 electron probe microanalyzer (EPMA) with a 20 kV accelerating voltage and 10 nA beam current after solution heat treatment. The C as well as Hf, B, and Zr contents of the experimental alloy ingots were determined by a high-frequency combustion infrared absorption method and inductively coupled plasma-atomic emission spectrometry (ICP-AES), respectively. Additionally, glow discharge optical emission spectroscopy (GDOES) was utilized to confirm the Si content of the master alloys. Taking the actual microstructure of the alloys under hot processing or servicing into consideration, two kinds of aging treatment were employed: (1) 1000 °C for 24 hours/312 hours/600 hours (air cooling); (2) 1050 °C for 4 hours + 900°C for 4 hours + 750 °C for 12 hours/ 312 hours/1000 hours/1500 hours (air cooling was used after each heat treatment). The γ/γ' two-phase compositions of the alloys after an aging heat treatment of 1000 °C for 600 hours and other phases were measured by a JXA8230 electron probe microanalyzer (EPMA) with a 20 kV accelerating voltage and 10 nA beam current.

The samples were prepared by a common method, and etched electrolytically in a solution of 42 mL H$_3$PO$_4$ + 32 mL H$_2$SO$_4$ + 24 mL H$_2$O. The γ/γ' microstructure was examined with a Zeiss GEMINI-SEM 500 field-emission scanning electron microscope (SEM) in different modes, and the equipped X-Max Extreme energy-dispersive X-ray spectroscopy (EDS) (Oxford Instruments), which possesses ultrahigh spatial resolution (~ 10 nm) and a high counting rate (10 times higher than that of the conventional EDS) was used to measure the phase compositions. The γ' area fraction and size were measured by the standard point count method and Image-Pro plus 6.0 software, respectively. The γ' volume fraction was assumed to be equal to the γ' area fraction for the sake of brevity. It should be pointed out that the γ' volume fraction may be slightly lower than the γ' area fraction. For each sample, no fewer than three images with their surface nearly parallel to {001} planes were used to obtain meaningful statistics (the total number of γ' was no less than 300, and the size of γ' was defined as the average length of diameters at 2 deg intervals and passing through the object's centroid by the Image-Pro plus 6.0 software).

The lattice constant of the γ and γ' phases of the experimental alloys after an aging treatment at 1000 °C for 600 hours was measured by the D/max 2550 diffractometer equipped with a CuKα1 monochromator at ambient temperature. A spinner stage and the spinning of the sample were applied to increase the counting rate. The curves were fitted using the Jandel scientific PeakFit computer program, and two pseudo-Voigt functions were used to obtain separate lattice constants for the γ and γ' phases. An FEI Tecnai G2 20 transmission electron microscope (TEM) was utilized to confirm the phase crystal structure and compositions, and a JEOL JEM-2100 transmission electron microscope was used for stacking fault analyses. TEM samples were prepared using a GL-696F ion-milled instrument. The equilibrium phase diagrams of the experimental alloys were calculated by the CALPHAD software Pandat combined with the latest Co-based database (PanCo-2019-TH), and this database contains 18 types of common elements except Hf. With the goal of improving the calculation accuracy, the calculation alloy compositions in this paper did not contain microelements except for Si.

III. RESULTS

A. *Effect of Al and Ti on Microstructural Stability at 1000 °C*

Figure 1 shows the backscatter electron (BSE) images containing the grain boundaries of the experimental

Table I. Compositions (At. Pct) and γ' Solvus Temperatures (°C) of Three Experimental Alloys[20]

Abbreviations	Co	Ni	Al	W	Mo	Ta	Ti
7Al-3.5Ti							
Nominal	bal.	30	7	2	1.5	1	3.5
Actual	bal.	30.08 ± 0.08	7.10 ± 0.05	2.04 ± 0.08	1.56 ± 0.11	1.03 ± 0.04	3.47 ± 0.12
5.5Al-4.2Ti							
Nominal	bal.	30	5.5	2	1.5	1	4.2
Actual	bal.	30.10 ± 0.04	5.59 ± 0.13	2.10 ± 0.05	1.60 ± 0.07	0.95 ± 0.11	4.31 ± 0.10
4Al-4.9Ti							
Nominal	bal.	30	4	2	1.5	1	4.9
Actual	bal.	30.04 ± 0.05	4.08 ± 0.10	1.98 ± 0.12	1.55 ± 0.09	1.04 ± 0.12	4.85 ± 0.08

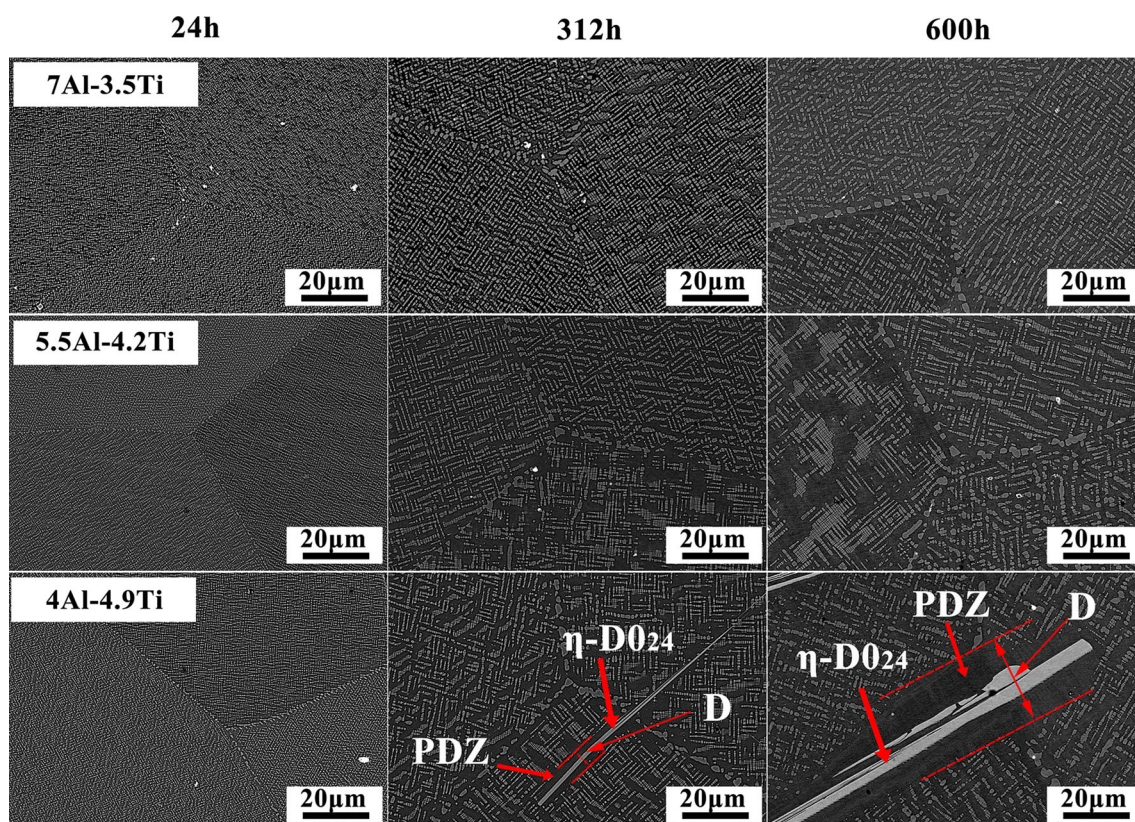| Abbreviations	Cr	Hf	C	Zr	B	Si	$T_{\gamma'}$
7Al-3.5Ti							
Nominal	12	0.100	0.080	0.010	0.080	0.400	1095
Actual	12.10 ± 0.10	0.110	0.080	0.009	0.085	0.390	
5.5Al-4.2Ti							
Nominal	12	0.100	0.080	0.010	0.080	0.400	1097
Actual	11.89 ± 0.18	0.110	0.071	0.009	0.085	0.390	
4Al-4.9Ti							
Nominal	12	0.100	0.080	0.010	0.080	0.400	1097
Actual	11.95 ± 0.16	0.100	0.070	0.010	0.090	0.410	

Fig. 1—Backscattered scanning electron microscope micrographs of the experimental alloys with a heat treatment of 1000 °C for 24 h/312 h/600 h.

alloys after solution and aging treatment at 1000 °C for 24 hours/312 hours/600 hours. The 7Al-3.5Ti and 5.5Al-4.2Ti alloys maintain a γ/γ' two-phase microstructure after an aging treatment of 1000 °C for 600 hours, and the white blocky precipitates in the grain interior are identified as MC carbides enriched in Hf,

Ta, and Ti. With decreasing Al(at. pct)/Ti(at. pct) in the experimental alloys, needle-like precipitates across grain boundaries appear in the 4Al-4.9Ti alloy after an aging treatment of 1000 °C for 312 hours, and there is a γ'-precipitate depleted zone (PDZ) near the larger end of that precipitate. With the extension of aging time, the precipitates grow along their length direction, and the average width (D) of the PDZ increases with increasing aging time. The EPMA results show that the main composition of the needle-like precipitates is 37.7Ni-35.6Co-11.0Ti-3.2Al-3.7Ta-3.1Cr-1.3Mo-3.3W (at. pct), which possesses a compositional characteristic of the $\eta(D0_{24})$-$(Co,Ni)_3Ti$ phase.

Figure 2 shows the locally magnified tips of the needle-like precipitates in the 4Al-4.9Ti alloy after an aging treatment of 1000 °C for 600 hours, revealing that the tip of the needle-like precipitates passes through the irregular γ', and no PDZ forms at the tip of that precipitates. The BSE image in Figure 2(b) shows that there is an obvious difference in the composition contrast between the γ' precipitates and its internal needle-like precipitates, while under the secondary electron (SE) mode, there is no obvious contrast difference between the two precipitates, as shown in Figures 2(c) and (d). The selected area electron diffraction obtained by TEM was used to identify the crystal structure and composition of the needle-like precipitates in the 4Al-4.9Ti alloy.

Figures 3(a) and (b) show TEM bright-field images of the 4Al-4.9Ti alloy containing the needle-like precipitates root and tip after a heat treatment of 1000 °C for 600 hours, respectively, and the insert SEM images in the upper right corner correspond to the TEM images of the needle-like precipitates. Figures 3(c) and (d) are selected area electron diffraction patterns (SADP) at positions A and B in Figures 3(a) and (b), respectively. Figures 3(e) and (f) represent the schematic diffraction patterns for Figures 3(c) and (d) respectively. It can be seen from the results that the needle-like precipitate is a η-$D0_{24}$ phase, and there exists a orientation relationship of $\langle 11\bar{2}0\rangle\{0001\}\eta\|\langle 110\rangle\{111\}\gamma/\gamma'$ between the coherent γ/γ'-$L1_2$ phase and the η-$D0_{24}$ phase. In addition, the composition analysis by TEM-EDS is the same as the results by SEM-EDS.

Figure 4 displays the morphology of the intragranular γ/γ' two phases for the experimental alloys after heat treatment of 1000 °C for 24 hours/312 hours/600 hours. The γ' volume fraction and size of heat-treated alloys calculated by Image-Pro Plus 6.0 software and the linear intercept method are shown in Table II. With prolonged aging time, the size of γ' precipitates gradually increases. From a comparative analysis of 7Al-3.5Ti, 5.5Al-4.2Ti and 4Al-4.9Ti alloys, it can be seen that the substitution of 0.7 at. pct Ti for 1.5 at. pct Al reduces the γ' volume fraction (this may be attributed to the replacement of 1.5 at. pct Al with 0.7 at. pct Ti decreasing the total content of γ' formers Al and Ti ((Al + Ti)at. pct)), and makes the size of the γ' first decrease and then slightly increase after aging at 1000 °C for 312 hours. After aging at 1000 °C for 600 hours, the cubic γ' precipitates for the 4Al-4.9Ti alloy become very irregular, which means that coherency has been lost at the γ/γ' interface. Therefore,
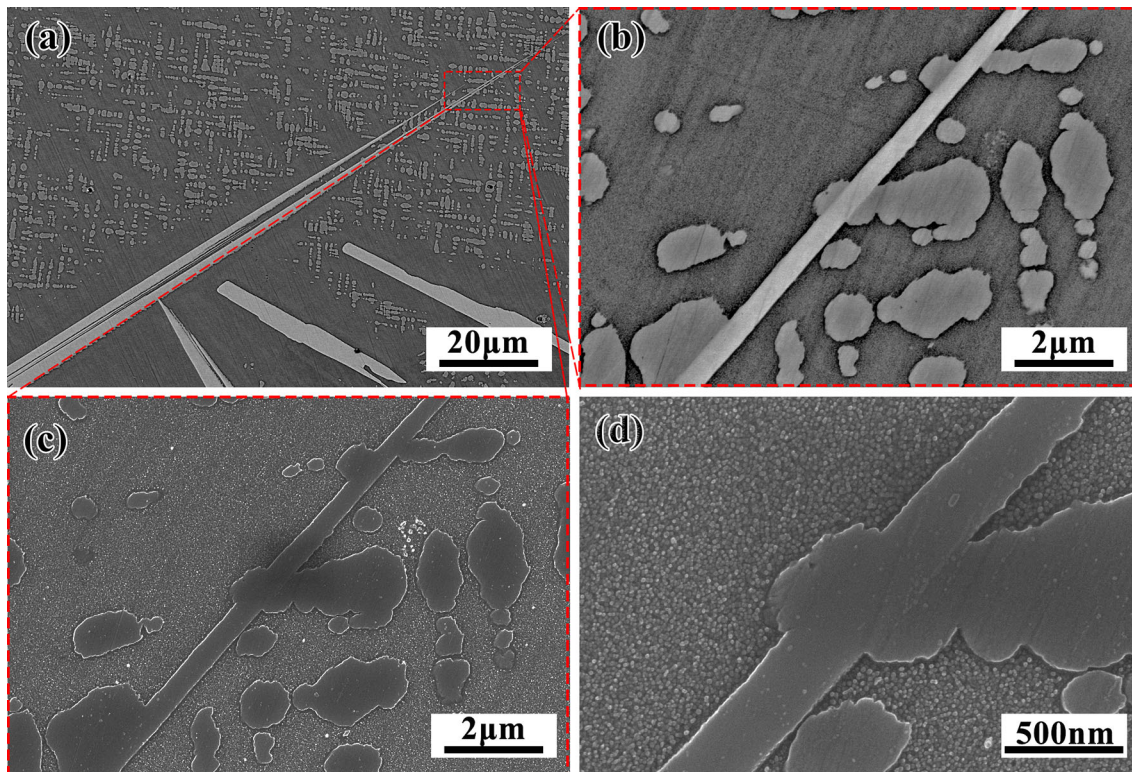

Fig. 2—The local magnification of the tip for the needle-like precipitates in the 4Al-4.9Ti alloy after an aging treatment of 1000 °C for 600 h. (*a*) × 1000 (BSE); (*b*) × 10,000 (BSE); (*c*) × 10,000 (SE); (*d*) × 30,000 (SE).
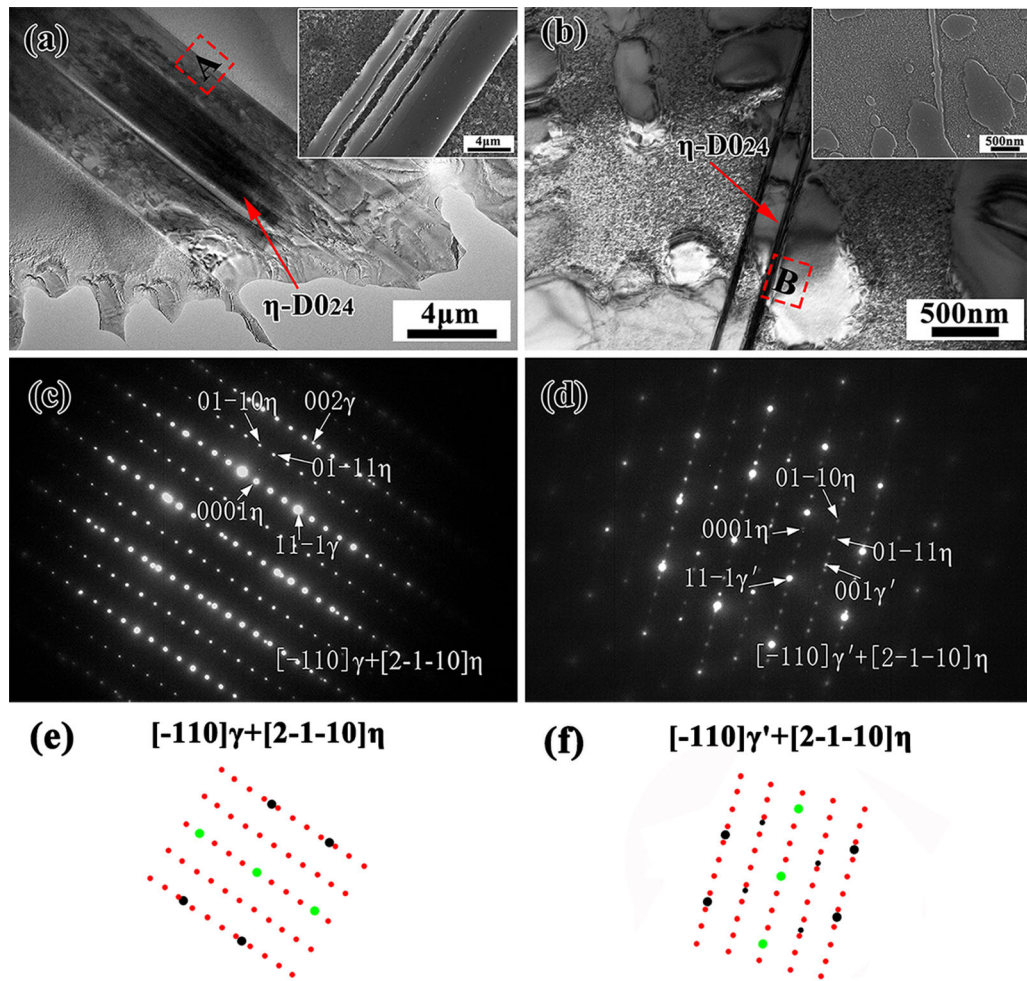
Fig. 3—TEM bright-field image of the 4Al-4.9Ti alloy containing the needle-like precipitate root (*a*) and tip (*b*) after a heat treatment of 1000 °C for 600 h; (*c*) and (*d*) are selected area electron diffraction patterns (SADP) at positions A and B in (a) and (b), respectively. (*e*) and (*f*) represent the schematic diffraction patterns for (c) and (d), respectively. The red circle represents the diffraction spot for η phase, the black circle represents the diffraction spot for γ or γ', and the green circle represents the overlapped diffraction spot.

the size of the γ' precipitates was not measured as shown in Table 2.

B. *Effect of Al and Ti on Microstructural Stability at 750 °C*

Figure 5 shows the backscatter electron (BSE) images containing the grain boundaries of the experimental alloys after solution and aging treatment at 1050 °C for 4 hours + 900 °C for 4 hours + 750 °C for 1500 hours. All alloys still show a γ/γ' two-phase microstructure without other detrimental phases after the abovementioned heat treatment, and the white blocky precipitates are presumed to be the MC carbides enriched in Ta, Ti, and Hf based on the compositional characteristics. This means that all the alloys possess good microstructural stability at 750 °C.

Figure 6 shows the secondary electron (SE) images with high magnification of the experimental alloys after solution and aging treatment of 1050 °C for 4 hours + 900 °C for 4 hours + 750 °C for 12 hours/312 hours/ 1000 hours/1500 hours. As is shown in Figure 6, all

alloys possess the γ' precipitates with a bimodal distribution, the larger type of γ' (> 100 nm) forms after aging at 1050 °C (named as primary γ'), and the smaller type of γ' (~ 50 nm) nucleates during air cooling after aging at 1050 °C for 4 hours and grows after aging at 900 °C (named as secondary γ'). The supersaturation of the experimental alloys during air cooling after aging at 1050 °C for 4 hours make the abovementioned smaller type of γ' nucleate during the cooling process (the relevant SEM images can refer to the Supplementary Figure S-1). The statistical γ' volume fraction and size are shown in Table III (To get the trustable area fraction for primary γ' from the microstructure shown in Figure 6, we used the BSE images which can refer to the Supplementary Figure S-2). A comparative analysis of 5.5Al-4.2Ti and 4Al-4.9Ti alloys shows that replacing 1.5 at. pct Al with 0.7 at. pct Ti leads to a slight decrease in the size of the γ' precipitates, especially for the primary γ' precipitates, and a much longer aging time above 1500 hours at 750 °C can make the size difference of primary γ' more evident. The effects of Al and Ti on the primary γ' precipitates volume fraction of the

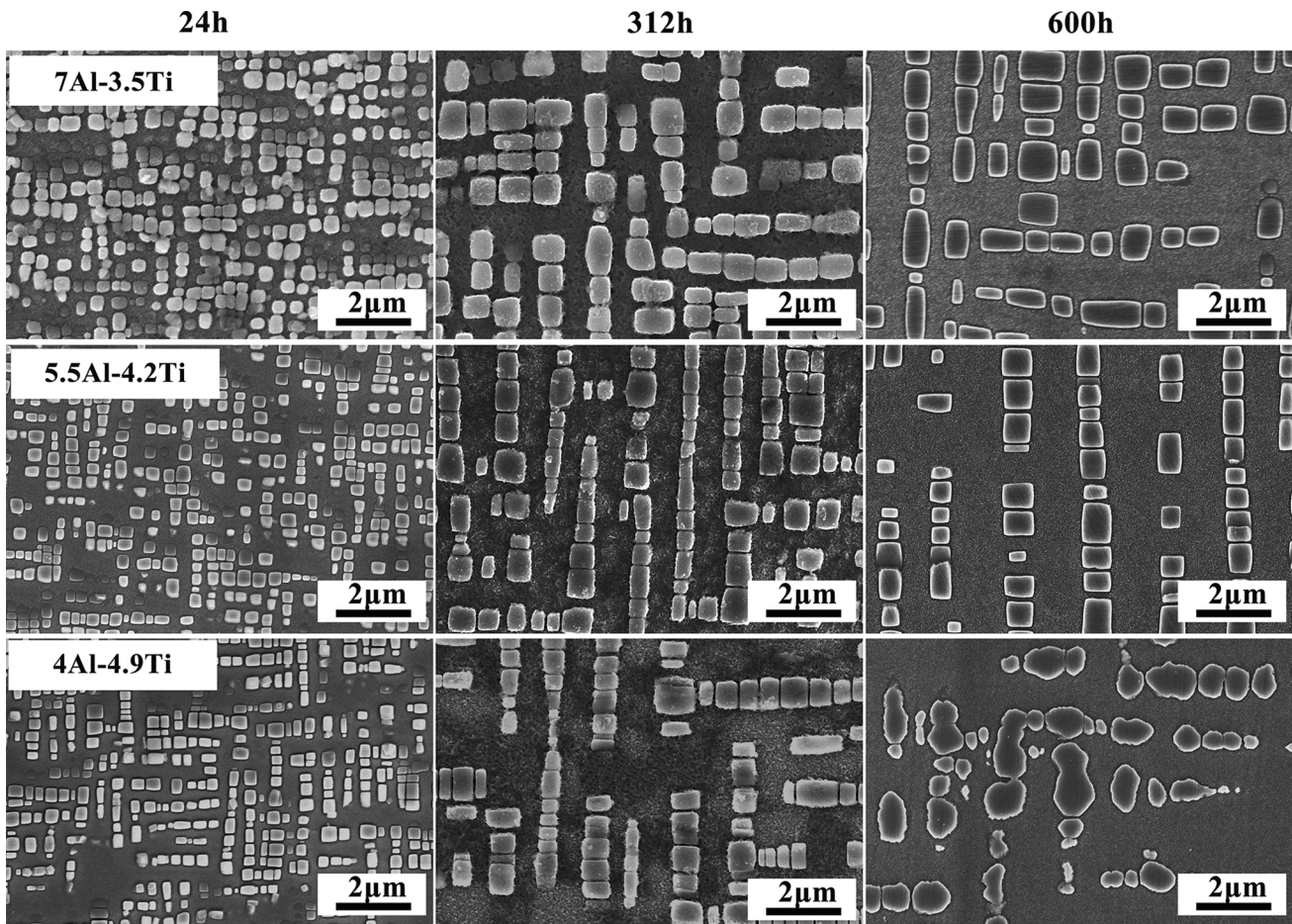|	24h	312h	600h

Fig. 4—Typical microstructure of γ' precipitates in the experimental alloys with an aging treatment of 1000 °C for 24 h/312 h/600 h.

experimental alloys are consistent with those obtained during aging at 1000 °C (Section III–A). The γ' size of the alloys gradually increases with prolonged aging time. In addition, some secondary γ' precipitates of the 4Al-4.9Ti alloy lose their cubic shape and grow along $\langle 001 \rangle$ direction after a heat treatment of 750 °C for 1000 hours, which is associated with the coalescence of γ' during the growth process. The coarsening behavior and coarsening mechanism of the γ' phase will be discussed in detail in Section IV–A.

C. Using Computational Thermodynamics to Predict the Effects of Al and Ti on Microstructural Stability

Accelerating the development of high-performance nickel-based superalloys using CALPHAD thermodynamics has been proved to be effective.[21] Because the validity of the thermodynamic database for the novel Co-based superalloys needs to be further verified by experiments, there are limited reports involving the CALPHAD thermodynamics in the alloy design process to date.[10,22]

Figure 7(a) shows an isopleth section equilibrium phase diagram of the alloy 46.33Co-30Ni-12Cr-1.5-Mo-0.4Si-2W-1Ta-6.77Ti-0Al (at. pct) when the 0.7 at. pct Ti is replaced by 1.5 at. pct Al calculated by the CALPHAD software Pandat combined with the latest Co-based database (PanCo-2019-TH). As shown in Figure 7(a), with increasing Al content and decreasing Ti content, there exists a transformation of the phase region at the multiphase region approximately 825 °C to 1080 °C, which refers to Fcc + $\eta \rightarrow$ Fcc + L1$_2\rightarrow$ B$_2$ + L1$_2$ + Fcc. Figures 7(b) through (d) show the phase mole fraction as a function of temperature for the compositions corresponding to the red dotted lines (b) through (d), respectively. Comparing the calculation results in Figures 7(b) through (d), it can be seen that the substitution of 0.7 at. pct Ti for 1.5 at. pct Al reduces the volume fraction of the γ'-L1$_2$ phase at 1000 °C and 750 °C, which is consistent with the statistical results shown in Tables II and III. In addition, the replacement of 1.5 at. pct Al with 0.7 at. pct Ti can keep the γ' solvus temperature almost unchanged, which is consistent with our previous report.[20]

However, in terms of the predication accuracy for long-term microstructural stability, the calculation results shown in Figure 7 of 7Al-3.5Ti and 4Al-4.9Ti alloys have some differences from the experimental results, except for the 5.5Al-4.2Ti alloy. The calculation results indicate that the 7Al-3.5Ti alloy will form a sigma (σ) phase at 750 °C (a typical representative component is (Cr$_{0.5}$Mo$_{0.1}$)(Co$_{0.2}$Ni$_{0.2}$)) and that the

Table II.   The Size and Volume Fraction of γ' Precipitates for Experimental Alloys After a Heat Treatment of 1000 °C for 24 h/ 312 h/600 h

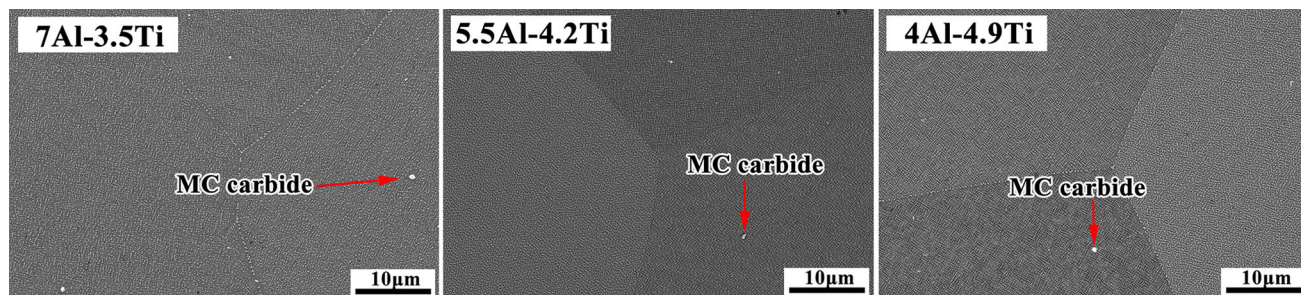|	Volume Fraction (Pct)			Size (nm)		
Abbreviations	24 h	312 h	600 h	24 h	312 h	600 h
7Al-3.5Ti	40.6 ± 2.1	38.6 ± 1.7	36.9 ± 3.2	236.5 ± 9.20	573.5 ± 15.6	699.1 ± 20.4
5.5Al-4.2Ti	35.7 ± 1.8	33.9 ± 2.3	30.5 ± 1.8	222.5 ± 19.2	522.6 ± 21.2	654.7 ± 18.6
4Al-4.9Ti	34.2 ± 2.5	31.4 ± 1.6	26.0 ± 3.0	215.5 ± 11.6	550.3 ± 7.90	—

Fig. 5—Backscattered scanning electron microscope micrographs of the experimental alloys with a heat treatment of 1050 °C for 4 h + 900 °C for 4 h + 750 °C for 1500 h.
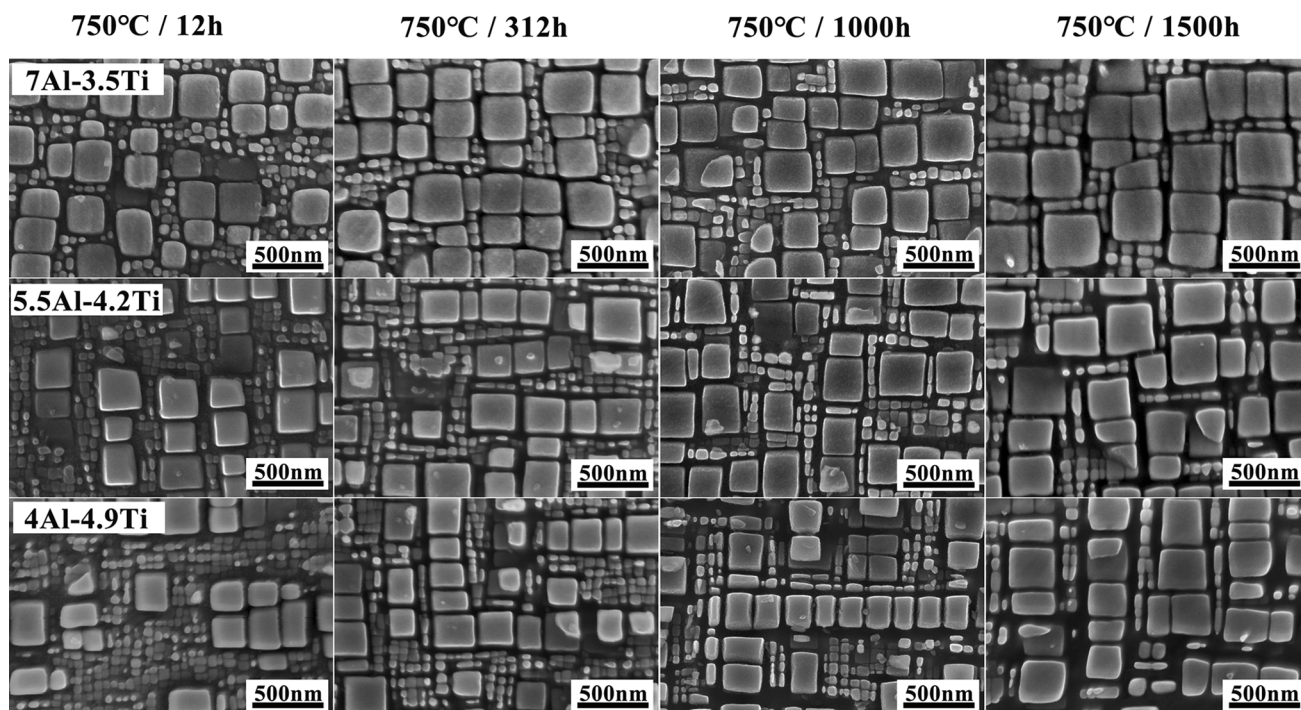

Fig. 6—The secondary electron (SE) images with high magnification of the experimental alloys after heat treatment at 1050 °C for 4 h + 900 °C for 4 h + 750 °C for 12 h/312 h/1000 h/1500 h.

equilibrium phase at 1000 °C for 4Al-4.9Ti alloy does not contain η-D0$_{24}$. Based on the experimental results, the three-phase region for Fcc + L1$_2$ + η in Figure 7(a) should move towards the direction of increasing Al content, *i.e.*, the intersection point A of the phase region in Figure 7(a) may move roughly to *A′*.

The abovementioned thermodynamic calculation results show that the Co-based database (Pan-Co-2019-TH) has good accuracy in predicting the γ' solvus of multicomponent Co-based superalloys and the effect of alloying elements on the γ' volume fraction. However, there are still some discrepancies in the

prediction of long-term microstructural stability. Higher accuracy for the thermodynamic calculation can be achieved by further improving the thermodynamic database.

D. *Effect of Al and Ti on the γ/γ′ Two-Phase Misfit*

The γ/γ′ two-phase misfit δ is an important parameter that influences microstructural stability, which is determined by the lattice constant of the γ phase (a_γ) and γ′ ($a_{\gamma'}$), as shown in Eq. [1].

$$\delta = \frac{2(a_{\gamma'} - a_\gamma)}{a_{\gamma'} + a_\gamma} \qquad [1]$$

Figure 8 shows the fitted diffraction curves of 7Al-3.5Ti, 5.5Al-4.2Ti, and 4Al-4.9Ti alloys, and the lattice misfit between the γ and γ′ phases can be determined by fitting the respective overall shape of the (002) peak for each alloy using pseudo-Voigt functions. Because the area ratio of the γ/γ′ two-phase diffraction peaks is proportional to its volume fraction ratio, the relative position of the two-phase diffraction peaks can be determined by the volume fraction shown in Table II. The actual lattice parameters for the γ and γ′ phases are also provided in Table IV. It can be seen from Table IV that substituting 0.7 at. pct Ti for 1.5 at. pct Al will increase the lattice constant of γ and γ′ at the same time, but the greater influence on the lattice parameter of γ′ makes the misfit values (δ) of the three experimental alloys increase. Analyzing the main reasons for the above change: Ti has a stronger effect on increasing the lattice parameters of γ or γ′ due to the larger atom radius of Ti (0.147 nm) compared with that of Al (0.143 nm).[23,24] The substitution of 0.7 at. pct Ti for 1.5 at. pct Al results in an increase in the content of Ti in γ and γ′, which may eventually lead to an increase in the lattice parameters of γ and γ′ at the same time. However, Ti is a γ′ former, which is mainly concentrated in γ′ as shown in Table IV, and the abovementioned partitioning behavior of Ti results in a greater impact on increasing the lattice parameters of γ′. Eventually, the composition change in γ′ and γ phases leads to the misfit variation of the experimental alloys.

The shape of the γ′ phase in Ni-base superalloys is closely related to the absolute value of misfit between the γ′ and γ′ phases [25]: the γ′ phase is formed as spheres at a 0 to 0.2 pct misfit, as cubes at about 0.5 to 1.0 pct and as plates at above about 1.25 pct. The cubic degree of the γ′ phase increases with increasing δ. The variation of the cubic degree of the γ′ phase for the experimental alloys shown in Table IV is consistent with the measured δ value.

IV. DISCUSSION

A. *The Coarsening Behavior of the γ′ Precipitate at 1000 °C and 750 °C*

The coarsening of the γ′ phase for the experimental alloys has different speeds after the heat treatment of 1000 °C for 24 hours/312 hours/600 hours and 1050 °C

for 4 hours + 900 °C for 4 hours + 750 °C for 12 hours/312 hours/1000 hours/1500 hours. The energy decrease of the total system containing all the γ′ phase provides the driven force for the growth of the γ′ phase. Extensive research shows that the coarsening of the γ′ phase in superalloys follows the classical Lifshitz–Slyozov–Wagner (LSW) theory,[26,27] although some assumptions remain for the LSW theory, including: a low volume fraction of precipitates, near zero solubility of solute atom in the matrix, no precipitate-precipitate interaction, a stationary coarsening process with almost unchanged γ′ volume fraction. The special expression is shown in Eq. [2].

$$r^n(t) - r_0^n(t) = Kt \qquad [2]$$

where r_0 is the initial precipitate radius, r is the instantaneous precipitate radius, K is the coarsening rate constant, and n is the temporal exponent. For volume diffusion-limited coarsening, which is often encountered, $n = 3$, while $n = 2$ when the interface reaction is the rate limiting process.[28]

The experimental data for aging at 1000 °C are used as an example to determine the temporal exponent for the experimental alloys. Figure 9(a) shows the plot of log (r, nm) as a function of log (t, s), and the fitted slopes of the curves corresponding to $1/n$ are 0.34 and 0.33 for the 7Al-3.5Ti and 5.5Al-4.2Ti alloys, respectively. These values are almost the same as the theory value $1/3$ (the γ′ precipitate coarsening is controlled by the diffusion of solutes in the matrix), which means that the γ′ phase coarsening of the experimental alloys is controlled by the diffusion of solutes in the matrix. The data for the 4Al-4.9Ti alloy are not shown in Figure 9(a) due to its irregular γ′ precipitates after aging at 1000 °C for 600 hours.

The third power of the mean precipitate radius (r^3) (defined as half of the average edge length of the cuboidal precipitates) follows a linear function of aging time (t) at 1000 °C and 750 °C in the experimental alloys, as shown in Figure 9(b). The slopes of fitting lines are coarsening rate coefficients (K), and the values of K for 7Al-3.5Ti, 5.5Al-4.2Ti and 4Al-4.9Ti alloys are listed in Table V. Moreover, the value of K for the secondary γ′ precipitates at 750 °C is listed in Table V. Comparing the K values at different temperatures, it can be seen that temperature is one of the most important factors affecting the coarsening of the γ′ phase. The variations of K for two different scales γ′ precipitates (primary and secondary γ′ precipitates) at 750 °C also show that the initial size for the γ′ precipitates has a significant effect on its coarsening.

From comparative analysis of coarsening rate constants at 1000 °C for the experimental alloys, the replacement of 1.5 at. pct Al with 0.7 at. pct Ti causes the coarsening rate constants of γ′ to first decrease and then slightly increase. Analyzing the main reason for the variations of K, the LSW rate constant K can be determined as shown in Eq. [3][29]:

$$K = \frac{8D_1 C\Gamma V_m}{9RT} \qquad [3]$$

Table III. The Size and Volume Fraction of γ′ Precipitates for Experimental Alloys After a Heat Treatment at 1050 °C for 4 h + 900 °C for 4 h + 750 °C for 12 h/312 h/1000 h/1500 h

Marks	Volume Fraction (Pct) (Primary)				Size (nm) (Primary)			
	12 h	312 h	1000 h	1500 h	12 h	312 h	1000 h	1500 h
7Al-3.5Ti	26.7 ± 1.5	34.3 ± 3.5	35.2 ± 2.1	37.8 ± 3.4	217.2 ± 10.9	252.3 ± 20.1	288.4 ± 7.6	316.6 ± 12.1
5.5Al-4.2Ti	23.2 ± 3.1	30.6 ± 2.3	32.9 ± 3.2	33.5 ± 1.3	210.5 ± 10.4	245.0 ± 12.1	278.8 ± 13.6	293.3 ± 17.1
4Al-4.9Ti	21.5 ± 2.6	27.1 ± 1.8	31.8 ± 1.2	32.9 ± 2.5	199.7 ± 13.2	228.1 ± 8.2	251.6 ± 10.2	270.7 ± 13.9

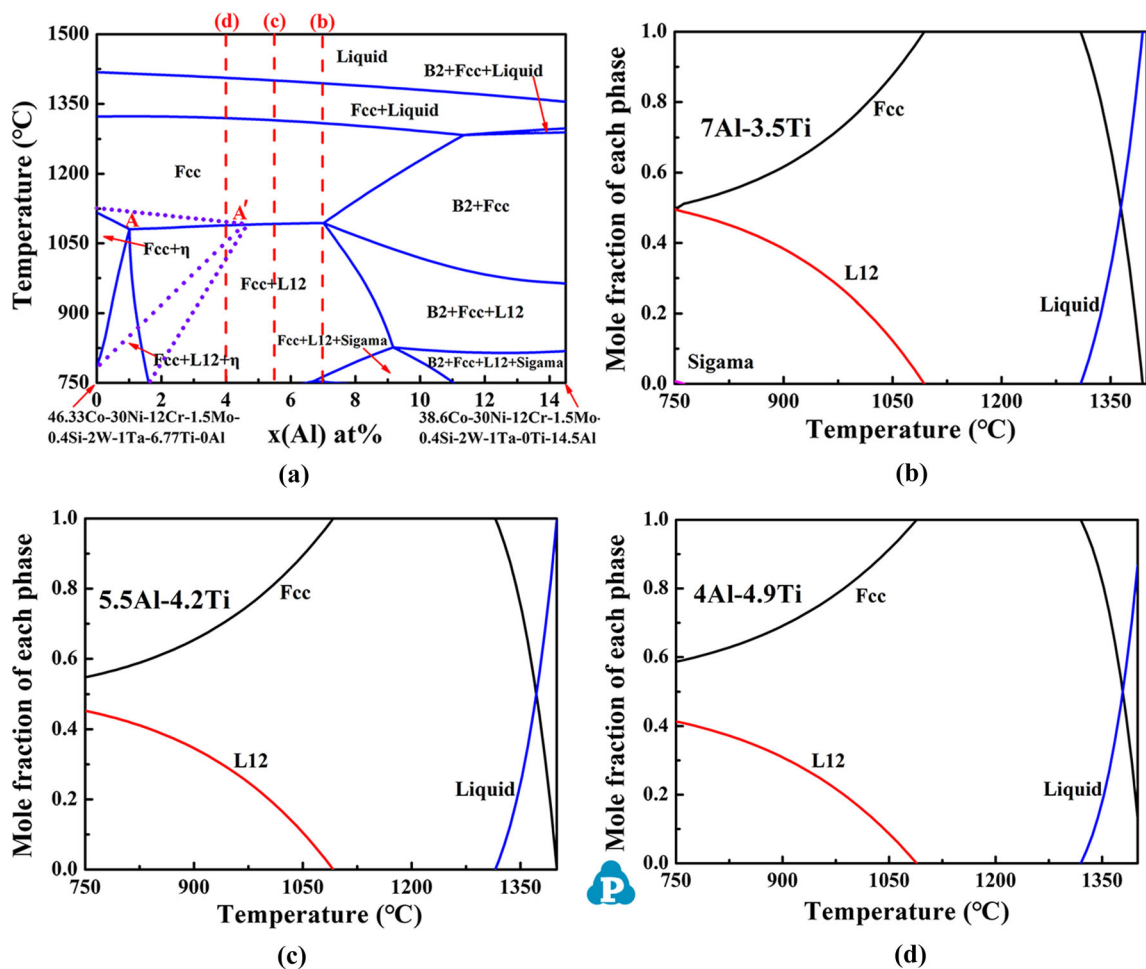| Marks	Size (nm) (Secondary)			
	12 h	312 h	1000 h	1500 h
7Al-3.5Ti	50.7 ± 3.6	60.4 ± 4.2	77.1 ± 3.0	86.6 ± 6.8
5.5Al-4.2Ti	47.2 ± 4.7	54.6 ± 3.2	71.0 ± 4.1	80.0 ± 5.1
4Al-4.9Ti	45.8 ± 2.6	60.5 ± 2.1	72.2 ± 3.7	83.1 ± 4.9

Fig. 7—The isopleth section equilibrium phase diagram of the alloy 46.33Co-30Ni-12Cr-1.5Mo-0.4Si-2W-1Ta-6.77Ti-0Al (at. pct) when the 0.7 at. pct Al is replaced by the 1.5 at. pct Al (*a*); (*b*), (*c*), and (*d*) show the phase mole fraction as a function of temperature for the compositions corresponding to the red dotted lines (b), (c), and (d) shown in (a), respectively. The blue dot line in (a) roughly represents the movement of the phase region based on the experimental results (Color figure online).

where, Γ is the surface energy associated with the γ/γ' interface, $D_1 = D_0 \exp\left(-\frac{Q}{RT}\right)$ is the temperature-dependent diffusion coefficient of the rate-controlling solute in the matrix, C is the equilibrium atomic fraction of that solute in the matrix, V_m is the molar volume of the precipitate, R is the ideal gas constant
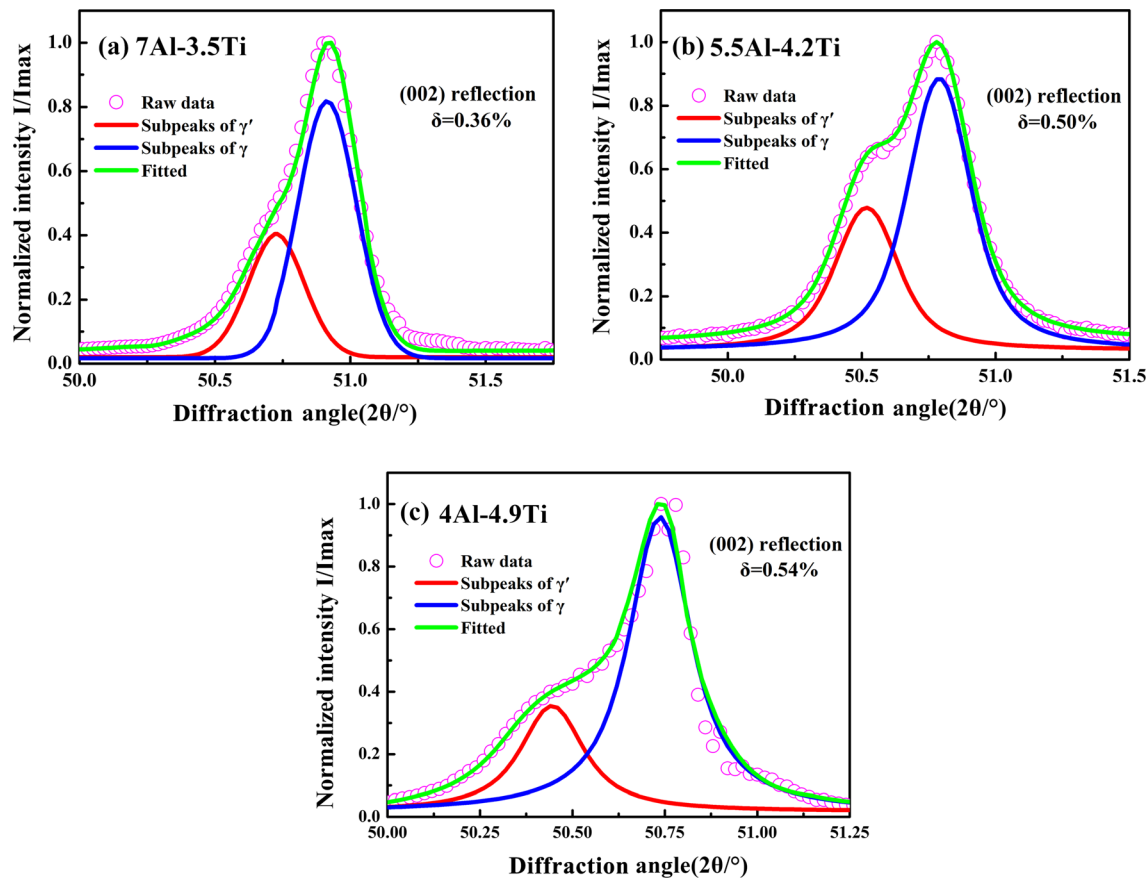
Fig. 8—XRD reflections of the experimental alloys with aging at 1000 °C for 600 h, (a) 7Al-3.5Ti, (b) 5.5Al-4.2Ti, (c) 4Al-4.9Ti.

(8.314 J K^{-1} mol^{-1}), and T is the absolute temperature.

As described in Eq. [3], the γ/γ' two-phase interfacial energy Γ and the diffusion coefficient of the solutes are important parameters that influence the coarsening behavior of γ' precipitates. For the coherent interface of the γ/γ' two phases, the interfacial energy decreases with the reduction of the misfit. Some studies suggest that the diffusion of Al in the matrix serves as the rate-controlling step in γ' coarsening in some Ni-based superalloys,[29–31] in which γ'-Ni$_3$Al is the brief expression of the strengthening phase. In the novel Co-Al-W-based superalloys, the research shows that the γ' coarsening was controlled by the diffusion of γ'-former W in the matrix which has a low diffusion rate.[32]

A comparative analysis of 7Al-3.5Ti and 5.5Al-4.2Ti alloys for coarsening rate coefficients K at 1000 °C shows that the 5.5Al-4.2Ti alloy exhibits higher δ, as shown in Figure 8, which leads to Γ(5.5Al-4.2Ti) > Γ(7Al-3.5Ti), whereas K(5.5Al-4.2Ti) < K(7Al-3.5Ti). Therefore, the interfacial energy Γ is not the main factor affecting the coarsening of γ' for 7Al-3.5Ti and 5.5Al-4.2Ti alloys. Other parameters may play a major role in deciding the K values. Meanwhile, based on Eq. [3], the diffusion coefficient (D_1) also plays an important role in deciding the K values. The diffusion coefficients (D_1) of the alloying elements at 1000 °C

which have been displayed in Table VI are calculated by using the Arrhenius equation (Eq. [4]):

$$D_1 = D_0 \exp\left(-\frac{Q}{RT}\right) \qquad [4]$$

where R is the ideal gas constant (8.314 J K^{-1} mol^{-1}), T is the absolute temperature, and Q and D_0 are the diffusion activation energy and frequency factor, respectively, obtained from the reference.[33]

Therefore, we assumed that the γ'-formers of Al, W, Ta, and Ti control the γ' coarsening of 7Al-3.5Ti and 5.5Al-4.2Ti alloys, respectively, and calculated the interfacial energies of the γ/γ' two phases by using the coarsening rate coefficients K in Table V and Eq. [3] (V_m was calculated using the lattice constants of γ' shown in Table IV, and the relevant calculation method can be referred to.[34] The diffusion coefficients (D$_1$) of the alloying elements in γ-Co at 1000 °C in Table VI were used, and the equilibrium atomic fraction (C) of the solute in the matrix refers to [20]): Al control: 124.6 Mj m^{-2}, 131.0 mJ m^{-2}; W control: 5810.7 mJ m^{-2}, 4805.5 mJ m^{-2}; Ta control: 2133.1 mJ m^{-2}, 1499.5 mJ m^{-2}; Ti control: 166.6 mJ m^{-2}, 107.9 mJ m^{-2}. The calculated interfacial energy when considering Al as a coarsening control element is comparable with that of common wrought Ni-base superalloys with high Al and Ti contents (50 mJ m^{-2} to 100 mJ m^{-2}),[35] and the relative magnitude of interfacial energy for 7Al-3.5Ti

Table IV.   Lattice Parameters of γ and γ′, Content of Al and Ti in γ/γ′ Two Phases and Misfits (δ) for the Experimental Alloys After Aging at 1000 °C for 600 h

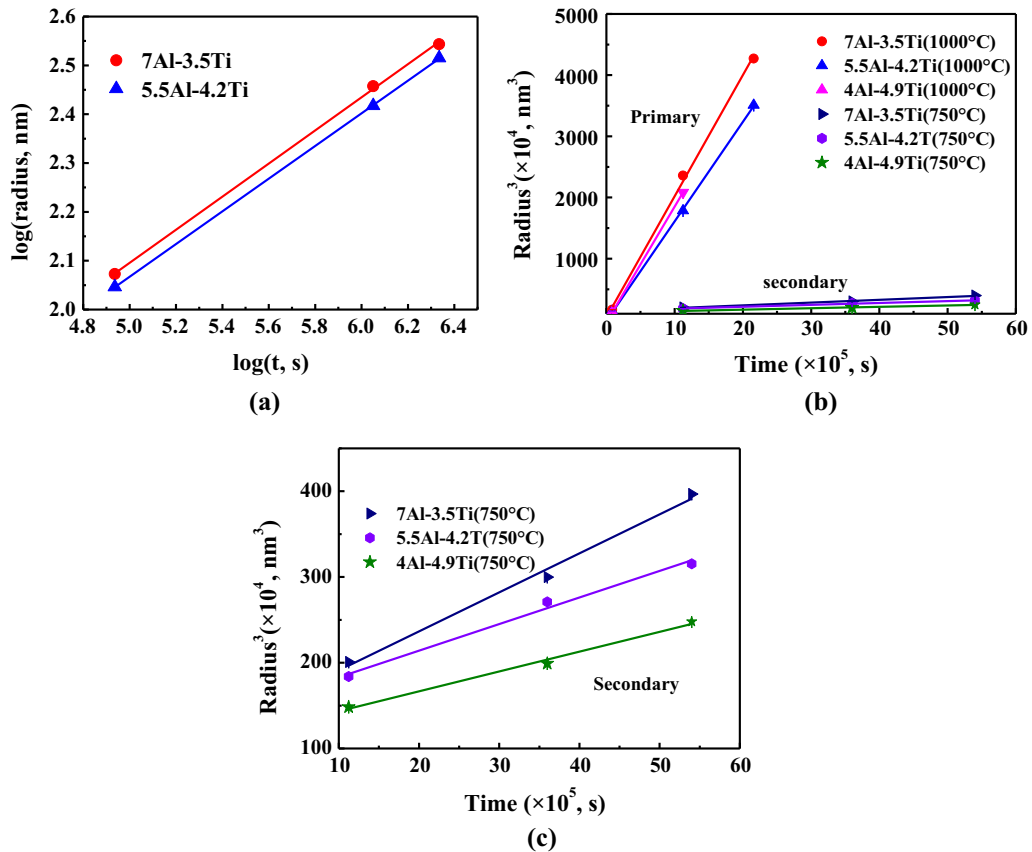| Alloy | Content of Al and Ti in γ′ and γ′ | | | | Lattice Diameter(nm) | | Misfit |
| | γ | | γ′ | | | | |
	Al (At. Pct)	Ti (At. Pct)	Al (At. Pct)	Ti (At. Pct)	γ	γ′	δ (Pct)
7Al-3.5Ti	6.42 ± 0.10	2.85 ± 0.18	9.94 ± 0.12	5.19 ± 0.65	0.35857	0.35985	0.36
5.5Al-4.2Ti	4.97 ± 0.08	3.58 ± 0.11	7.98 ± 0.13	7.17 ± 0.40	0.35940	0.36120	0.50
4Al-4.9Ti	3.75 ± 0.08	3.89 ± 0.03	6.55 ± 0.07	9.92 ± 0.27	0.35975	0.36169	0.54

Fig. 9—The plot of log (r, nm) as a function of log (t, s) during aging at 1000 °C (a), and the third power of the mean precipitate radius (r^3) (defined as half of the average edge length of the cuboidal precipitates) vs aging time (t) during aging at 750 °C (primary γ′) and 1000°C (b); (c) is the enlargement of the curve in (b) for the secondary γ′.

Table V.   The Coarsening Rate Coefficients K (m^3s^{-1}) of γ′ at the Aging Temperature for 750 °C and 1000 °C

Temperature	7Al-3.5Ti	5.5Al-4.2Ti	4Al-4.9Ti
1000 °C	1.98×10^{-26}	1.63×10^{-26}	1.89×10^{-26}
750 °C (Primary γ′)	0.0455×10^{-26}	0.031×10^{-26}	0.0231×10^{-26}
750 °C (Secondary γ′)	0.0125×10^{-27}	0.0102×10^{-27}	0.0101×10^{-27}

and 5.5Al-4.2Ti alloys (Γ(5.5Al-4.2Ti): 124.6 mJ m^{-2} > Γ(7Al-3.5Ti): 131.0 mJ m^{-2}) is consistent with that determined by the relative magnitude of misfit δ shown in Table 4. From the point of diffusion alone, the diffusion coefficient of Ti in γ-Co shown in Table VI is higher than that of Al at 1000 °C, but increasing the

content of Ti leads to a slight decrease of the coarsening rate coefficients K for the 5.5Al-4.2Ti alloy. According to Eq. [3], it can infer that the effect of Ti on the coarsening process may also not be stronger than that of Al for 7Al-3.5Ti and 5.5Al-4.2Ti alloys. The abovementioned discussion indicates that Al may play a major role in the process of γ' phase coarsening. In addition, Γ(4Al-4.9Ti) $> \Gamma$(5.5Al-4.2Ti) may make K(4Al-4.9Ti) $>$ K(5.5Al-4.2Ti).

By analyzing the coarsening rate coefficients K of the experimental alloy at 750 °C shown in Table V, it can be seen that the substitution of 0.7 at. pct Ti for 1.5 at. pct Al will lead to a gradual slight decrease in the γ' phase coarsening rate, especially for the primary γ' precipitates. Compared with the 5.5Al-4.2Ti alloy, the 4Al-4.9Ti alloy has a higher misfit δ, but it exhibits a lower γ' coarsening rate for the primary γ' precipitates at 750 °C. However, the γ' coarsening rate at 1000 °C for the 4Al-4.9Ti alloy is slightly higher than that of the 5.5Al-4.2Ti alloy. The main reasons for the abovementioned variation of K are as follows: the higher γ' volume fraction and more narrow γ phase channel aging at 750 °C compared with aging at 1000 °C may result in a more obvious elastic interaction between the coherent stress field arising from the coherent precipitates (the magnitude of coherent stress between γ/γ' two phases has positive correlation with the misfit δ), and the higher coherent stress field may inhibit the γ' coarsening[36,37] (the coherent stress field between the γ phase and γ' phase on the coarsening of γ' is not considered in the traditional LSW theory). Eventually, the highest misfit δ for the 4Al-4.9Ti alloy may result in the lowest γ' coarsening rate at 750 °C. In addition, the γ' coarsening behavior at 750 °C for the 7Al-3.5Ti and 5.5Al-4.2Ti alloys which possess smaller coherent stress may be similar to that at 1000 °C.

As described in the abovementioned results and discussions, the difference of the γ' coarsening behavior at 1000 °C and 750 °C is attributed to the interaction of the interfacial energy, diffusion of the solute atoms, and coherent stress. Moreover, it can be referred that the coarsening behavior of γ' in the medium temperature range for the novel wrought Co-based superalloys containing the important strengthening elements Ta and Ti may be strongly affected by its high misfit δ.

B. The Formation Mechanism of $\eta(D0_{24})$-$(Co,Ni)_3Ti$

Our previous study shows that the mechanical properties of the novel wrought Co-based superalloys can be obviously improved by adjusting the relevant content of Al and Ti on the premise of maintaining a large processing window and good hot deformation property,[20] but 4Al-4.9Ti alloy with a higher Ti(at. pct)/Al(at. pct) value forms needle-like $\eta(D0_{24})$-$(Co,Ni)_3Ti$ after aging at 1000 °C for 312 hours. The needle-like $\eta(D0_{24})$-$(Co,Ni)_3Ti$ enriched γ'-formers such as Ti, Ta, and W can decrease the γ'-phase strengthening and deteriorate the creep and fatigue properties. It is important to clarify its formation mechanism for guiding alloy composition design.

Comparing the compositions of γ', γ[20] and η-$D0_{24}$ shown in Table VII, the element Ti is a decisive element for the formation of the η phase. The content of Ti in the η and γ' phases is very high, while the content of Ti in the γ phase is 3.89 at. pct. Such a low content of Ti does not seem to satisfy the requirement of direct nucleation and growth of $\eta(D0_{24})$-$(Co,Ni)_3Ti$ in γ the matrix. Figure 10 shows the TEM bright-field image of the 4Al-4.9Ti alloy after aging at 1000 °C for 600 hours. It can be seen in Figure 10 that there are some stacking faults in γ' after aging at 1000°C for 600 h, and dislocation networks shown in Figure 10(c) exist at the interface between the γ/γ' two phases. Some stacking faults pass through the whole γ' phase, and some stacking faults do not pass through the whole γ' phase, with a Shockley superpartial dislocation remaining in γ', as shown in Figure 10(b). Moreover, there exist stacking faults in γ' adjacent to $D0_{24}$ needles (marked by red arrow in Figure 10(d)), which indicates that the stacking faults seem to be connected with the γ'-L1$_2$ to η-$D0_{24}$ phase transformation (In order to eliminate the possible influence of the fringes on the observation, the figure for the TEM images at the same location with different tilt angle can refer to the Supplementary Figure S-3). The formation of the stacking faults in γ' and the dislocation networks at the interface between γ/γ' two phases in the 4Al-4.9Ti alloy may be related to the release of coherency stress during the aging heat treatment.

Based on the results shown in Figure 10, the morphology shown in Figure 2, the compositions shown in Table 7 and the orientation relationship between η/γ' two phases for $\langle 11\bar{2}0\rangle\{0001\}\eta\|\langle 110\rangle\{111\}\gamma'$ shown in Figure 3, it can be inferred that $\eta(D0_{24})$-$(Co,Ni)_3Ti$ may nucleate by shearing of the γ', and then grows up through element diffusion, resulting in a large PDZ at the root and almost no PDZ at the tip of the η phase.

The specific shear deformation process is shown in Figure 11. First, the γ'(L1$_2$)-$(Ni,Co)_3(Al,Ti,W)$ phase has an ordered FCC structure, and its {111} atomic planes are stacked by ABCABCABC... (where A, B, and C represent the {111} plane). The unit cell structure of γ' is shown in Figure 11(a); $\eta(D0_{24})$-$(Co,Ni)_3Ti$ has an ordered HCP structure, and its unit cell structure is shown in Figure 11(b). When two adjacent {111} planes in the γ' successively slip along the $1/3\langle 11\bar{2}\rangle$ Burgers vector, the stacking mode for the close-packed {111} will become ABCACBCABC..., i.e., the formation of a superlattice extrinsic stacking fault (SESF). The abovementioned process means that an initial core of $D0_{24}$ structure forms, and the local stacking mode for the close-packed {111} is CACBC as shown in Figure 11(c). If such a mechanism operates after every two {111} atomic layers, then L1$_2$ will be transformed into $\eta(D0_{24})$. Finally, the two phases form the orientation of $\langle 11\bar{2}0\rangle\{0001\}\eta\|\langle 110\rangle\{111\}\gamma'$.

From the perspective of energy, the increase of Ti (at. pct)/Al (at. pct) may reduce the SESF energy of the experimental alloys, which provides a driving force for the transformation from L1$_2$ to $D0_{24}$ for 4Al-4.9Ti alloy (this expression also means that the high ratio of Ti (at. pct)/Al (at. pct) would stabilize η with respect to γ',

Table VI. The Calculated Diffusion Coefficients of Different Alloying Elements in γ-Co at 1000 °C

Alloying Elements	Al	W	Ta	Ti	Cr	Mo
Interdiffusion Coefficients(D_1)/m^2 s^{-1} ($\times$ 10^{-17})	105	7.61	69.1	177	32.4	35.5

Table VII. Compositions (At. Pct) of γ′, γ[20] and η(D0$_{24}$) Phases Measured by EPMA in 4Al-4.9Ti Alloy After Aging at 1000 °C for 600 h

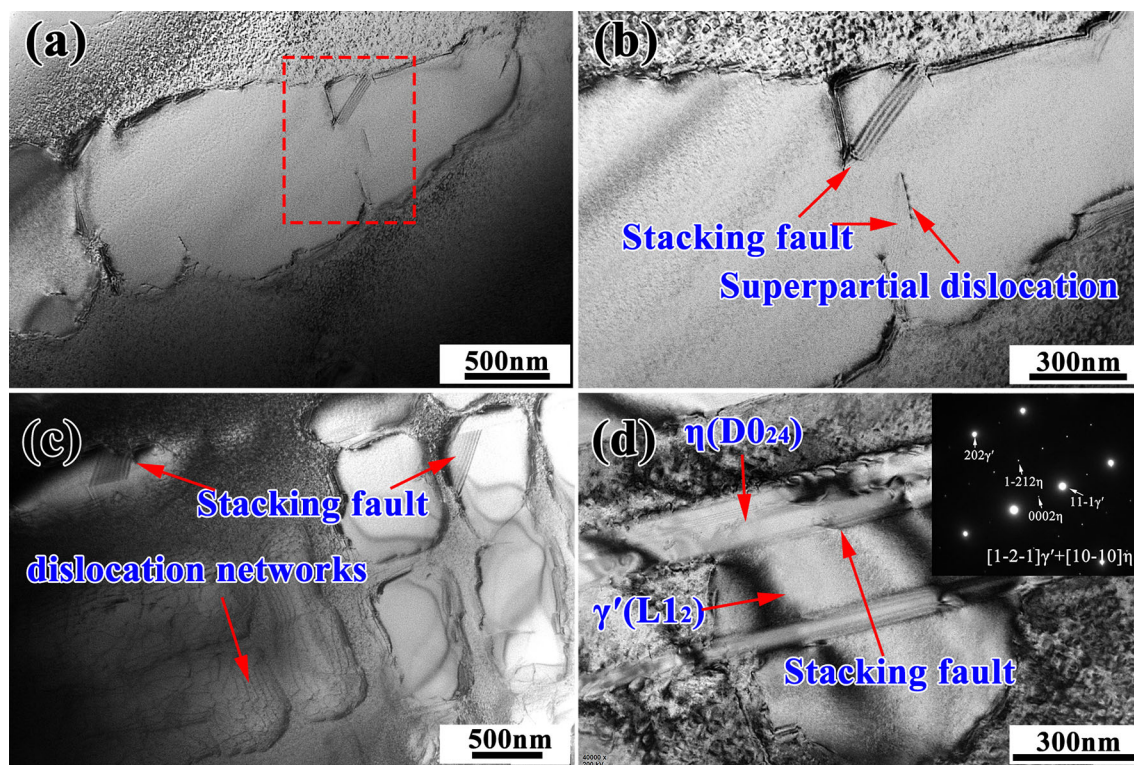| Precipitations	Co	Al	W	Ta	Ti	Cr	Ni	Mo
η(D0$_{24}$)	bal.	3.2 ± 0.2	3.3 ± 0.1	3.7 ± 0.2	11.0 ± 0.2	3.1 ± 0.1	37.7 ± 1.2	1.3 ± 0.2
γ′(L1$_2$)	bal.	6.6 ± 0.1	2.2 ± 0.1	1.9 ± 0.2	9.9 ± 0.3	4.6 ± 0.6	38.2 ± 0.6	0.8 ± 0.2
γ	bal.	3.75 ± 0.1	1.86 ± 0.1	0.63 ± 0.0	3.89 ± 0.0	13.97 ± 0.1	27.66 ± 0.1	1.72 ± 0.1

Fig. 10—Representative TEM bright-field image of 4Al-4.9Ti alloy after aging at 1000°C for 600 h (a), (b), (c), and (d). (b) is the high magnification of the position shown in the red rectangle of (a) (Color figure online).

which is similar to that in Ni-based superalloys[38]). In addition, during the aging heat treatment of the Ni-Ti binary alloy, there also exist a transformation from γ′-L1$_2$ to η-D0$_{24}$ along with a thin η phase (5 nm) forming in the γ′.[39] For the Co-Al-W ternary alloy, the transformation of the γ′-L1$_2$ phase to that of the χ-DO$_{19}$ phase during aging at 900 °C was facilitated by the movement of superpartial dislocations, and the stacking faults were identified as the initial step of the decomposition of the γ′-L1$_2$ phase.[17]

Although the transformation from γ′-L1$_2$ to η-(D0$_{24}$) can be accomplished by glide of 1/3⟨11$\bar{2}$⟩{111} Shockley partial dislocations, the composition of the two phases remains basically unchanged after this transformation. At this time, diffusion plays an important role in its growth process. Table VII shows the specific compositions of η-(D0$_{24}$) and γ′-(L1$_2$) in the 4Al-4.9Ti alloy after the heat treatment at 1000 °C for 600 hours. It can be seen that the formation and growth of η(D0$_{24}$)-(Co,-Ni)$_3$Ti requires the diffusion of Ta, Ti, Mo, and W to the η phase as well as the diffusion of Al and Cr to the γ′-(L1$_2$) phase. As the growth of η-(D0$_{24}$) consumes a large number of γ′-formers such as Ti and
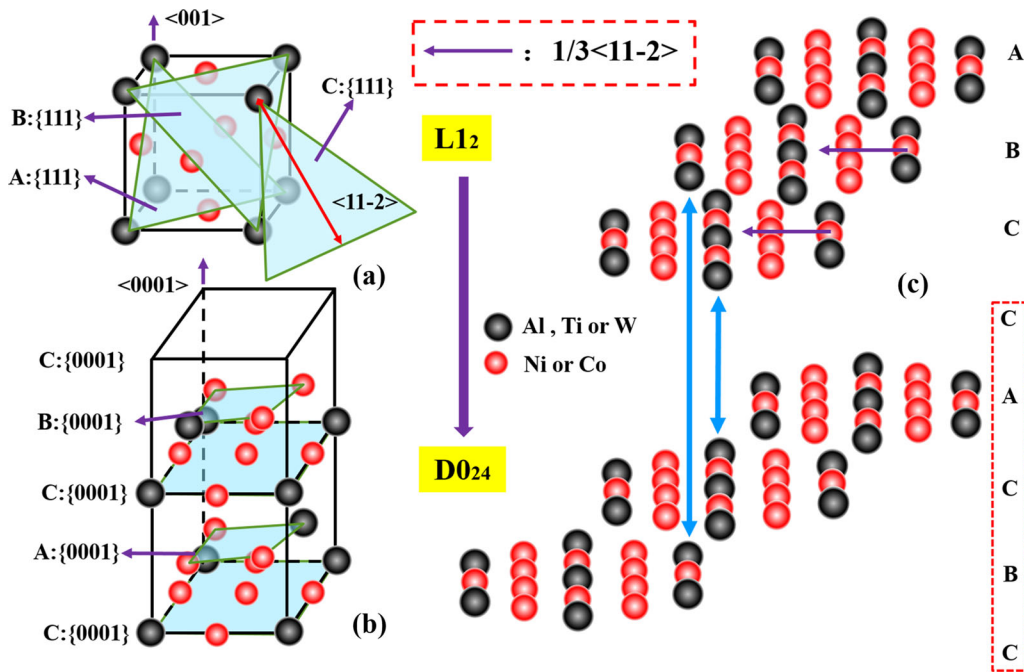
Fig. 11—Atomic arrangement in a unit cell of $L1_2$ (a) and $D0_{24}$ (b), and the schematic of atomic layer movement for the transformation from $L1_2$ to $D0_{24}$ by glide of $1/3\langle11\bar{2}\rangle\{111\}$ Shockley partial dislocations (c).
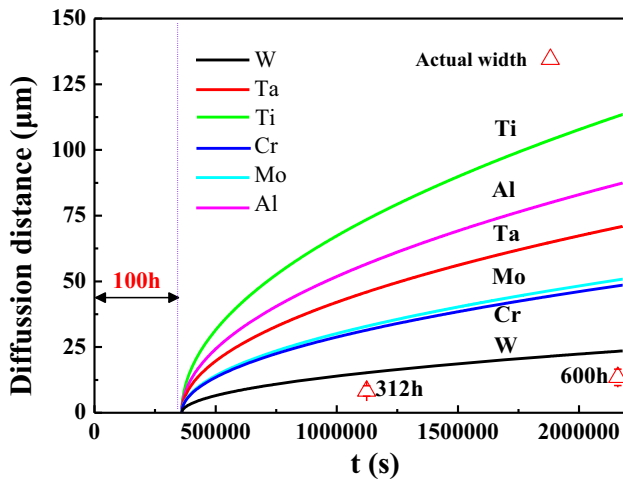

Fig. 12—The diffusion distance of each element at 1000 °C in the 4Al-4.9Ti alloy calculated using the standard volume diffusion equation $\langle x \rangle = 2\sqrt{D_1 t}$,[40] and the actual average width of the PDZ as shown in Fig. 1.

Ta, the PDZ will form at the larger end of η-($D0_{24}$), as shown in Figure 1.

In this paper, the width increase of PDZ is accompanied by diffusion, so the width (D) of PDZ can be used to evaluate the role of different alloy elements in the diffusion process. Without considering the effect of alloy element concentration on the diffusion coefficient, the diffusion distance of each element in the 4Al-4.9Ti alloy is calculated using the standard volume diffusion equation $\langle x \rangle = 2\sqrt{D_1 t}$,[40] where x is the diffusion distance and D_1 displayed in Table 6 is the diffusion coefficient of different alloy elements in γ-Co at 1000 °C, as shown in

Figure 12. In fact, the test time for examining the formation of η-($D0_{24}$) in 4Al-4.9Ti alloy is discrete, and the actual time for the formation of η-($D0_{24}$) is difficult to determine. In addition to the microstructure shown in Figure 1, there is still no formation of η-($D0_{24}$) in 4Al-4.9Ti alloy after aging at 1000 °C for 100 hours (the SEM micrograph is not shown here). Therefore, it roughly assumes that the η-($D0_{24}$) phase forms after aging at 1000 °C for 100 hours in Figure 12.

Table VIII shows the diffusion distance d of different alloying elements in γ-Co at 1000 °C, as well as the actual average width of the PDZ (defined as $d = D/2$) as shown in Figure 1. From the analysis of Table VIII and Figure 12, it can be inferred that the growth of PDZ may be mainly controlled by W, and the low diffusion coefficient of W in γ-Co at 1000 °C may restrict the growth of η-$D0_{24}$.

Compared with the results shown in Section IV–A that Al may play a major role in the process of γ' phase coarsening, the important effect of W on η-$D0_{24}$ growth indicates that the coarsening of γ' may be essentially different from the formation of η-$D0_{24}$. In fact, as described in the abovementioned discussion, the formation of η-$D0_{24}$ involves the transformation from γ'-$L1_2$ to η-$D0_{24}$, and the energy difference between the two structures can provide a driving force for this transformation. Titus et al.[41] reported that the segregation of the W element at SISFs in novel Co- and CoNi-based superalloys can make the part of γ' obtain a lower energy configuration and promote the formation of SISFs and Co_3W-$D0_{19}$. Moreover, Smith et al.[42] have shown that some alloying elements exhibit different element segregation behavior between SISF ($D0_{19}$) and SESF ($D0_{24}$) during the creep process for the

Table VIII. The Calculated Diffusion Distance d of Different Alloying Elements in γ-Co at 1000 °C, As Well As the Actual Width of the PDZ (Defined as $d = D/2$), as Shown in Fig. 1

Alloying Elements	Diffusion Distance $d/\mu m$	
	312 h	600 h
Al	56.6	87
W	15.2	23.4
Ta	45.9	70.5
Ti	73.6	113
Cr	31.5	48.3
Mo	32.9	50.5
Actual Width	8.3 ± 2.0	13.5 ± 3.1

high-performance wrought nickel-based superalloy (LSHR), recently. For element W, it is enriched at SISF and SESF. However, the concentration increment of element W (defined as: $\Delta C_W = C_W(\text{SESF or SISF}) - C_W(\gamma')$, C_W represents the concentration of W) at SESF is greater than that at SISF. This result may partly reflect the fact that element W tends to be further enriched in SESF. In this study, the enrichment of the W element in η-$D0_{24}$ may be beneficial for the formation of η-$D0_{24}$, and eventually, the growth of η-$D0_{24}$ may be mainly controlled by the diffusion of W.

In Ni-based superalloys, a similar PDZ with the width d at the grain boundary resulting from the titanium diffusion to the carbides shows a linear function of $t^{1/2}$.[43] Meanwhile, the width of the PDZ at the grain boundary resulting from the tungsten diffusion to the borides also shows a linear dependence on $t^{1/2}$ in Co-based superalloys.[44] The abovementioned reports show the importance of alloy element diffusion on the formation of PDZ. In this study, the interaction of multicomponent alloy elements and the underestimation of the formation time for η-($D0_{24}$) may make the measured width of the PDZ smaller than that controlled by the diffusion of W.

V. SUMMARY AND CONCLUSION

The microstructural evolution of multicomponent γ'-strengthened Co-based superalloys at 750 °C and 1000 °C with different Al and Ti contents was investigated. The following conclusions can be drawn:

(1) With the increase of Ti (at. pct)/Al (at. pct) for the experimental alloys, 4Al-4.9Ti alloy formed $\eta(D0_{24})$-$(Co,Ni)_3Ti$ after aging at 1000 °C for 312 hours, but the 7Al-3.5Ti and 5.5Al-4.2Ti alloys still maintain a γ/γ' two-phase microstructure after a heat treatment of 1000 °C for 600 hours. All the alloys possess a good intermediate-temperature microstructure stability, which have γ/γ' two phases after aging at 750 °C for 1500 hours.

(2) The growth of the $\eta(D0_{24})$-$(Co,Ni)_3Ti$ phase is controlled by the diffusion of W, and the γ'-$L1_2$ and $\eta(D0_{24})$-$(Co,Ni)_3Ti$ phases exhibit the following OR: $\langle 11\bar{2}0\rangle\{0001\}\eta\|\langle 110\rangle\{111\}\gamma'$.

(3) The substitution of 0.7 at. pct Ti for 1.5 at. pct Al can lead to an increase of Ti at. pct in γ' phase, which leads to an increase of the γ/γ' two-phase misfits for the experimental alloys.

(4) When aging at 1000 °C, the γ' coarsening is controlled by the diffusion of solute atoms in the matrix. The replacement of 1.5 at. pct Al with 0.7 at. pct Ti will cause the coarsening rate of γ' phase to first decrease and then increase. However, when aging at 750 °C, the substitution of 0.7 at. pct Ti for 1.5 at. pct Al lead to a gradual decrease in the γ' coarsening rate, especially for primary γ'. The increase of the coherence stress field between γ/γ' two phases caused by the increase of misfit δ may eventually result in a lower γ' coarsening rate of 4Al-4.9Ti alloy than that of 5.5Al-4.2Ti alloy.

ELECTRONIC SUPPLEMENTARY MATERIAL

The online version of this article (https://doi.org/10.1007/s11661-020-05652-0) contains supplementary material, which is available to authorized users.

REFERENCES

1. J. Sato, T. Omori, K. Oikawa, I. Ohnuma, R. Kainuma, and K. Ishida: *Science*, 2006, vol. 312, pp. 90–1.
2. T.M. Pollock, J. Dibbern, M. Tsunekane, J. Zhu, and A. Suzuki: *JOM*, 2010, vol. 62, pp. 58–63.
3. M. Tsunekane, A. Suzuki, and T.M. Pollock: *Intermetallics*, 2011, vol. 19, pp. 636–43.
4. K. Shinagawa, T. Omori, J. Sato, K. Oikawa, I. Ohnuma, R. Kainuma, and K. Ishida: *Mater. Trans.*, 2008, vol. 49, pp. 1474–79.
5. F. Xue, H.J. Zhou, Q.Y. Shi, X.H. Chen, H. Chang, M.L. Wang, and Q. Feng: *Scr. Mater.*, 2015, vol. 97, pp. 37–40.
6. G. Feng, H. Li, S.S. Li, and J.B. Sha: *Scr. Mater.*, 2012, vol. 67, pp. 499–502.
7. M. Ooshima, K. Tanaka, N.L. Okamoto, K. Kishida, and H. Inui: *J. Alloy. Compd.*, 2010, vol. 508, pp. 71–78.
8. F. Pyczak, A. Bauer, M. Göken, U. Lorenz, S. Neumeier, M. Oehring, J. Pual, N. Schell, A. Schreyer, A. Stark, and F. Symanzik: *J. Alloy. Compd.*, 2015, vol. 632, pp. 110–15.
9. L. Klein, A. Bauer, S. Neumeier, M. Göken, and S. Virtanen: *Corros. Sci.*, 2011, vol. 53, pp. 2027–34.
10. W. Li, L. Li, S. Antonov, and Q. Feng: *Mater. Des.*, 2019, vol. 180, p. 107912.
11. S. Neumeier, L.P. Freund, and M. Göken: *Scr. Mater.*, 2015, vol. 109, pp. 104–107.

12. L.P. Freund, S. Giese, D. Schwimmer, H.W. Höppel, S. Neumeier, and M. Göken: *J. Mater. Res.*, 2017, vol. 32, pp. 1–8.
13. M. Knop, P. Mulvey, F. Ismail, A. Radecka, K.M. Rahman, T.C. Lindley, B.A. Shollock, M.C. Hardy, M.P. Moody, T.L. Martin, P.A.J. Bagot, and D. Dye: *JOM*, 2014, vol. 66, pp. 2495–501.
14. Y. Zhang, H.D. Fu, X.Z. Zhou, Y.H. Zhang, and J.X. Xie: *Mater. Sci. Eng. A*, 2018, vol. 737, pp. 265–273.
15. C.H. Zenk, S. Neumeier, H.J. Stone, and M. Göken: *Intermetallics*, 2014, vol. 55, pp. 28–39.
16. P.J. Bocchini, C.K. Sudbrack, R.D. Noebe, D.C. Dunand, and D.N. Seidman: *Mater. Sci. Eng. A*, 2017, vol. 705, pp. 122–32.
17. Y.Z. Li, F. Pyczak, M. Oehring, L. Wang, J. Paul, U. Lorenz, and Z.K. Yao: *J. Alloy. Compd.*, 2017, vol. 729, pp. 266–76.
18. N. Volz, C.H. Zenk, R. Cherukuri, T. Kalfhaus, M. Weiser, S.K. Makineni, C. Betzing, M. Lenz, B. Gault, S.G. Fries, J. Schreuer, R. Vaßen, S. Virtanen, D. Raabe, E. Spiecker, S. Neumeier, and M. Göken: *Metall. Mater. Trans. A*, 2018, vol. 49A, pp. 4099–109.
19. L.P. Freund, A. Stark, A. Kirchmayer, N. Schell, F. Pyczak, M. Göken, and S. Neumeier: *Metall. Mater. Trans. A*, 2018, vol. 49A, pp. 4070–78.
20. Y. Zhang, H.D. Fu, X.Z. Zhou, Y.H. Zhang, and J.X. Xie: *Intermetallics*, 2019, vol. 112, p. 106543.
21. C.J. Small and N. Saunders: *MRS Bull.*, 1999, vol. 24, pp. 22–26.
22. E.A. Lass: *Metall. Mater. Trans. A*, 2017, vol. 48A, pp. 2443–59.
23. H.-Y. Yan, J. Coakley, V.A. Vorontsov, N.G. Jones, H.J. Stone, and D. Dye: *Mater. Sci. Eng. A*, 2014, vol. 613, pp. 201–208.
24. W.F. Gale and T.C. Totemeier: *Smithells Metals Reference Book*, 8th ed., Elsevier, Amsterdam, 2004, pp. 4.44–4.77.
25. E.W. Ross and C.T. Sims: *Superalloys II*, A Wiley-Interscience Publication, New York, 1987, pp. 97–133.
26. I.M. Lifshitz and V.V. Slyozov: *J. Phys. Chem. Solids*, 1961, vol. 19, pp. 35–50.
27. C. Wagner: *Z. Elektrochem.*, 1961, vol. 65, pp. 581–91.
28. A.J. Ardell and V. Ozolins: *Nat. Mater.*, 2005, vol. 4, pp. 309–16.
29. J. Tiley, G.B. Viswanathan, R. Srinivasan, R. Banerjee, D.M. Dimiduk, and H.L. Fraser: *Acta Mater.*, 2009, vol. 57, pp. 2538–49.
30. M. Fährmann, E. Fährmann, T.M. Pollock, and W.C. Johnson: *Metall. Mater. Trans. A*, 1997, vol. 28A, pp. 1943–45.
31. G.S. Shin, J.Y. Yun, M.C. Park, and S.J. Kim: *Mater. Charact.*, 2014, vol. 95, pp. 180–186.
32. S. Meher, S. Nag, J. Tiley, A. Goel, and R. Banerjee: *Acta Mater.*, 2013, vol. 61, pp. 4266–76.
33. S. Neumeier, H.U. Rehman, J. Neuner, C.H. Zenk, S. Michel, S. Schuwalow, J. Rogal, R. Drautz, and M. Göken: *Acta Mater.*, 2016, vol. 106, pp. 304–12.
34. A.J. Ardell and R.B. Nicholson: *J. Phys. Chem. Solids*, 1966, vol. 27, pp. 1793–804.
35. T. Hara, S. Kobayashi, T. Ueno, and K. Oikawa: *J. Cryst. Growth*, 2019, vol. 506, pp. 91–96.
36. E. Balikci and D. Erdeniz: *Metall. Mater. Trans. A*, 2010, vol. 41A, pp. 1391–98.
37. R.S. Moshtaghin and S. Asgari: *Mater. Des.*, 2003, vol. 24, pp. 325–30.
38. C.Y. Cui, Y.F. Gu, D.H. Ping, and H. Harada: *Metall. Mater. Trans. A*, 2009, vol. 40A, pp. 282–91.
39. M. Kompatscher, B. Schönfeld, H. Heinrich, and G. Kostorz: *J. Appl. Cryst.*, 2000, vol. 33, pp. 488–91.
40. *Diffusion in Solid Metals and Alloys, Landolt-börnstein New Series, Gr III*, 8th ed., H. Mehrer, ed., *Diffusion in Solid Metals and Alloys, Landolt-börnstein New Series, Gr III*, Springer, Berlin, 1990, pp. 2–3.
41. M.S. Titus, A. Mottura, G.B. Viswanathan, A. Suzuki, M.J. Mills, and T.M. Pollock: *Acta Mater.*, 2015, vol. 89, pp. 423–37.
42. T.M. Smith, B.S. Good, T.P. Gabb, B.D. Esser, A.J. Egan, L.J. Evans, D.W. McComb, and M.J. Mills: *Acta Mater.*, 2019, vol. 172, pp. 55–65.
43. T. Krol, D. Baither, and E. Nembach: *Acta Mater.*, 2004, vol. 52, pp. 2095–108.
44. A. Bauer, S. Neumeier, F. Pyczak, R.F. Singer, and M. Göken: *Mater. Sci. Eng. A*, 2012, vol. 550, pp. 333–41.